Acta Biomaterialia 72 (2018) 110–120

Contents lists available at ScienceDirect

Acta Biomaterialia

journal homepage: www.elsevier.com/locate/actabiomat

Full length article

Melt electrowriting below the critical translation speed to fabricate crimped elastomer scaffolds with non-linear extension behaviour mimicking that of ligaments and tendons

Gernot Hochleitner [a,1], Fei Chen [b,1], Carina Blum [a], Paul D. Dalton [a], Brian Amsden [b], Jürgen Groll [a,*]

[a] Department of Functional Materials in Medicine and Dentistry and Bavarian Polymer Institute (BPI), University Hospital of Würzburg, Pleicherwall 2, 97070 Würzburg, Germany
[b] Department of Chemical Engineering and Human Mobility Research Centre, Queen's University, Kingston, Ontario K7L 3N6, Canada

ARTICLE INFO

Article history:
Received 24 October 2017
Received in revised form 4 March 2018
Accepted 9 March 2018
Available online 17 March 2018

Keywords:
Crimp structure
Biomimetic scaffolds
Toe region mechanical behaviour
Melt electrowriting (MEW)
Photo-cross-linkable elastomer

ABSTRACT

Ligaments and tendons are comprised of aligned, crimped collagen fibrils that provide tissue-specific mechanical properties with non-linear extension behaviour, exhibiting low stress at initial strain (*toe region* behaviour). To approximate this behaviour, we report fibrous scaffolds with sinusoidal patterns by melt electrowriting (MEW) below the critical translation speed (CTS) by exploitation of the natural flow behaviour of the polymer melt. More specifically, we synthesised photopolymerizable poly(L-lactide-co-ε-caprolactone-co-acryloyl carbonate) (p(LLA-co-ε-CL-co-AC)) and poly(ε-caprolactone-co-acryloyl carbonate) (p(ε-CL-co-AC)) by ring-opening polymerization (ROP). Single fibre (fØ = 26.8 ± 1.9 μm) tensile testing revealed a customisable *toe region* with Young's Moduli ranging from E = 29 ± 17 MPa for the most crimped structures to E = 314 ± 157 MPa for straight fibres. This toe region extended to scaffolds containing multiple fibres, while the sinusoidal pattern could be influenced by printing speed. The synthesized polymers were cytocompatible and exhibited a tensile strength of σ = 26 ± 7 MPa after 10^4 cycles of preloading at 10% strain while retaining the distinct toe region commonly observed in native ligaments and tendon tissue.

Statement of Significance

Damaged tendons and ligaments are serious and frequently occurring injuries worldwide. Recent therapies, including autologous grafts, still have severe disadvantages leading to a demand for synthetic alternatives. Materials envisioned to induce tendon and ligament regeneration should be degradable, cytocompatible and mimic the ultrastructural and mechanical properties of the native tissue. Specifically, we utilised photo-cross-linkable polymers for additive manufacturing (AM) with MEW. In this way, we were able to direct-write cytocompatible fibres of a few micrometres thickness into crimp-structured elastomer scaffolds that mimic the non-linear biomechanical behaviour of tendon and ligament tissue.

1. Introduction

Damaged ligaments and tendons are amongst the most common soft tissue injuries worldwide and thus, bear a high potential for advanced approaches in regenerative medicine [1]. Therapies to cure tendon and ligament ruptures still include the implantation of autologous grafts, which have serious drawbacks including limited availability, and frequent donor site morbidity or scar formation [2–4]. Hence, alternative approaches include using polymer scaffolds as biomaterials to substitute for the damaged tendon and ligaments [5–7]. With the recent advent of additive manufacturing (often termed 3D printing in the media), a greater variety of designs and manufacturing routes for medical biomaterials is now possible [8], to better mimic the biomechanical function of the original tissue [9].

Recapitulating the mechanical performance of ruptured tendons and ligaments using medical implants is very challenging.

* Corresponding author.
E-mail addresses: gernot.hochleitner@fmz.uni-wuerzburg.de (G. Hochleitner), chenf@queensu.ca (F. Chen), carina.blum@fmz.uni-wuerzburg.de (C. Blum), paul.dalton@fmz.uni-wuerzburg.de (P.D. Dalton), amsden@queensu.ca (B. Amsden), juergen.groll@fmz.uni-wuerzburg.de (J. Groll).
[1] Shared first authorships.

https://doi.org/10.1016/j.actbio.2018.03.023
1742-7061/

Tough, strong, stiff and creep-resistant materials are desired to mimic the biomechanical tensile behaviour of tendons and ligaments, which also have non-linear mechanical properties. Tendons and ligaments contain highly organized and aligned collagenous tissue that is capable of absorbing forces during locomotion [10]. Both tissues are organized in fascicles that are linearly oriented along the axis of the tissue. These fascicles contain fibres that are composed of collagen fibrils. The morphological characteristics of the fibres varies not only between ligaments and tendons but also within each of the tissues, depending on the exact location within the tissue. However, one important generic minimal functional and structural feature of the ultrastructure of both ligaments and tendons is the presence of crimped sub-micron-sized collagen fibrils. These crimped fibrils are usually referred to as the tissue typical biomechanically relevant morphological feature of tendons and ligaments, as the crimped morphology results in a non-linear, tensile stress-strain behaviour. During elongation up to ≈2% strain, the crimped fibrils become straightened accompanied by an increasing Young's modulus. This results in a characteristic toe region; further stretching produces a linear biomechanical region. In this linear region of the stress-strain curve, the ultrastructure becomes increasingly lengthened with more elongation until micro-failure processes start, ultimately resulting in rupture [11–13].

The non-linear biomechanics of tendon and ligament is to be recapitulated in this study using a direct-writing technology termed melt electrowriting (MEW) [14]. This technique utilizes strong electrical fields to deposit fibres onto planar or cylindrical collectors. Thin fibres with diameters previously ranging from 800 nm to 50 μm are formed and can be stacked on top of each other in a layer-by-layer or additive manufacturing approach [15–17]. Alternatively, when MEW is performed at collector speeds that are below the electrified jet speed, a buckling phenomenon of the jet occurs, similar to a column of honey falling onto toast [18]. Such mechanical buckling of a viscoelastic column produces an array of different patterns that can be modelled and predicted [18–20]. This buckling of the fluid enables the deposition of sinusoidal fibre structures [21] which we use to approximate the crimped collagenous fibrils in tendons and ligaments. In this case, a precise process control over the collector movement and melt jet speed is essential as small discrepancies can disturb the resulting scaffold design.

While poly(lactic-co-glycolic acid) (PLGA) or poly(ε-caprolactone) (PCL) are well known polymers used in 3D printing for tissue engineering applications, they are either subject to elongation due to creep and often exhibit a notable reduction in modulus upon hydration due to the plasticizing effect. These polymers are thermoplastic – and not elastomeric – and thus, undergo plastic deformation even at small strains. Recently, we demonstrated MEW of a UV-cross-linkable polymer, poly(L-lactide-co-ε-caprolactone-co-acryloyl carbonate) (p(LLA-ε-CL-AC)), to fabricate strong, stiff, elastic and creep-resistant fibre scaffolds, even under wet conditions [22]. However, this polymer lacked a stable deposition performance, a suitable lifetime of the melt in the MEW reservoir at elevated temperatures as well as accurate stacking properties and is therefore not suitable for controlled fabrication of sinusoidal structured scaffolds.

To overcome this challenge, we synthesized a different UV-cross-linkable polymer, poly(ε-caprolactone-co-acryloyl carbonate) (p(ε-CL-AC)), and investigated its printability via MEW in comparison to p(LLA-ε-CL-AC). In order to demonstrate its cytocompatibility, an eluate test with L929 murine fibroblasts based on DIN EN ISO 10993-5:2009, as well as adhesion tests and live/dead-staining using human mesenchymal stem cells (hMSC) were performed. Furthermore, a controlled sinusoidal printing approach to fine-tune the sinusoid morphology of was demonstrated. The resulting tensile tests on single fibres and scaffolds indicated that aligned, crimped and mechanically robust elastomeric scaffolds which mimic the nonlinear stress-strain response of natural ligaments and tendons can be obtained by combining photo-cross-linkable poly(CL-AC) with MEW.

2. Materials and methods

L-lactic acid (LLA), (Purac, The Netherlands) was purified by recrystallization from dried toluene. ε-caprolactone (ε-CL), purchased from Lancaster, Canada, was dried over calcium hydride and distilled under vacuum and stored over activated 4 Å molecular sieves. The acryloyl carbonate (AC) monomer was synthesised using a previously described protocol [23]. Stannous 2-ethylhexanoate ($Sn(Oct)_2$, 96% purity), 1-octanol, and anhydrous toluene were obtained from Sigma-Aldrich (Ontario, Canada) and used as received. Dichloromethane (DCM) and methanol were obtained from Fisher Scientific, Canada.

2.1. Polymer preparation

The copolymers were synthesized by ring-opening polymerization according to a previously published protocol [22]. The LLA, CL and AC monomers were polymerised in anhydrous toluene at 115 °C for 24 h using $Sn(Oct)_2$ as a catalyst and 1-octanol as an initiator with LLA:CL:AC target molar ratios of 65:25:10 (referred as PLACLAC) and 0:90:10 (referred as PCLAC), as shown in Fig. 1. The reaction mixture was then cooled and precipitated in cold methanol and re-dissolved in 5 mL of DCM and precipitated in cold methanol for another two cycles and finally dried under vacuum at room temperature for 3 days. The polymer was then kept in a 20 mL glass vial protected under a N_2 atmosphere at −20 °C and wrapped with aluminium foil until use.

Prior to use, the thermally resistant photo-initiator Irgacure 651 (2,2-dimethoxy-2-phenylacetophenone, Sigma-Aldrich Co, St. Louis, USA) was added to each batch of polymer. A concentration of 1% w/w was achieved by mixing the Irgacure 651 with DCM at a ratio of 1:1 (blend [g]:solution [1 mL]), then evaporating the solvent under a steady flow of air in a fume food. The solid blend was manually mixed again to assure a proper dispersion. The whole blending procedure was conducted excluding direct irradiation with natural or artificial light.

2.2. Polymer characterization

The composition of the copolymers was calculated from the ^{1}H-NMR spectra obtained in $CDCl_3$ on a Bruker Avance 400 MHz with peak shifts referenced using an internal tetramethylsilane standard. The composition was calculated by comparing the integration of the characteristic peaks from LLA (CH, δ = 5.1 ppm), ε-CL (CH_2, δ = 2.26 ppm) and AC units (vinyl protons, δ = 5.5–6.5 ppm).

The number average molecular weight (M_n) and molar mass dispersity ($Đ_M$) of the copolymers were characterized by gel permeation chromatography (GPC) using a Waters 2695 GPC apparatus with a guard and 4 columns, and a Waters 410 Differential Refractometer. Samples were dissolved in HPLC grade tetrahydrofuran (THF) at 3 mg/mL and filtered with a 0.2 μm syringe filter. THF was used as the eluent at a flow rate of 0.3 mL/min and polystyrene standard was used.

A Mettler Toledo DSC1 system was used to measure the thermal properties (glass transition temperature (T_g), melting point (T_m), and heat of fusion (ΔH_f)) of the synthesized copolymers. The samples were run at a heating and cooling rate of 10 °C/min using the

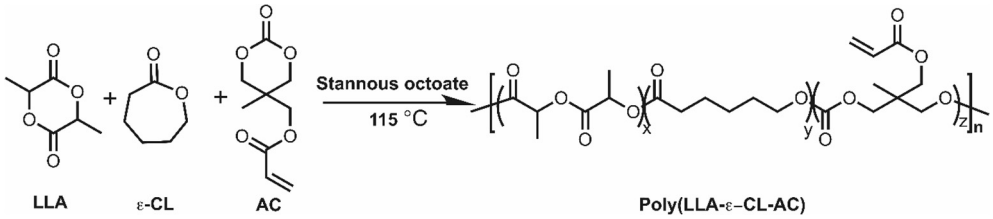

Fig. 1. Schematic of ROP. LLA, ε-CL and AC react to poly(L-lactide-co-ε-caprolactone-co-acryloyl carbonate) (p(ε-CL-co-AC)).

following temperature program. The sample was first cooled from 25 °C to −80 °C and held for 1 min at that temperature. This cycle was followed by heating from −80 to 160 °C with a hold time of 1 min at 160 °C. It was further cooled from 160 to −80 °C with a hold time of 1 min at −80 °C. Finally, the sample was heated from −80 to 160 °C. The glass transition temperature was obtained from the inflection point of the second heating cycle. The minimum of the endothermic curve in the first heating cycle was taken as T_m, while the area bound by the endotherm normalised to mass of the polymer sample was used to calculate ΔH_f.

2.3. Processing via MEW

A custom-built MEW printer was used, described elsewhere [22]. To ensure a maximum lifetime of the molten polymer in the printhead reservoir, a minimum MEW temperature T_{min} leading to a homogenous fibre deposition was assessed and used in this study. Thereby the nozzle and reservoir temperature were increased in +5 °C increments until a continuous and homogeneous jet with a sufficient speed of approximately ≥100 mm/min was achieved. Afterwards, the reservoir temperature T_{res} was lowered to increase the processing lifetime of the polymer. Only changes in T_{res} that had no distinct influence on the MEW performance were conducted.

Fibre arrays were manufactured with increasing collector speeds of +5 and +12 mm/min speed steps to determine the CTS. The CTS is a specific collector speed that matches the molten jet speed impinging the moving surface [15] and is the point where the direct-written fibre transforms from sinusoidal to linear morphology.

The effect of different feeding pressures of 0.3, 0.5, 1.0, 2.0 and 4.0 bar on CTS and deposited fibre diameters (fØ) was studied. For these experiments, the acceleration voltage U = 7.0 kV and collector distance l = 4.5 mm were kept constant. To facilitate a proper optical analysis, transparent and electrical conductive glass slides coated with indium-tin-oxide (50 × 50 mm^2, Adafruit Industries, New York, USA) were used as a collector surface. MEW was conducted until the polymer could no longer be processed. The lifetime of a single print was characterized with n = 5, the complete array printing experiments were repeated with n = 2 for PLACLAC and with n = 4 for PCLAC. For the mechanical testing, single fibres and scaffolds were printed.

In order to demonstrate the structural precision and for cytocompatibility testing, box-structured scaffolds with straight fibres and a mesh width of 200 μm in x- and y-direction were printed using a 30 G nozzle at p = 1.0 bar, U = 7.0 kV, l = 4.5 mm and a collector speed of 300 mm/min. A total number of 10 layers, 5 in x- and 5 in y- direction, were alternately stacked.

Further, for sinusoidal scaffolds the settings U = 5.5 kV and p = 4.0 bar were used. Therefore, sinusoidal-shaped fibres were printed with a velocity under CTS in x-direction with a distance of 250 μm in between and a stacking of three fibres above each other. Straight fibres were printed with a velocity above CTS every 10 mm in y-direction as support structure in between of two sinusoidal fibre layers in x-direction. Hence, the sinusoidal scaffolds consisted of 6 layers in total, 3 sinusoidal-shaped layers in x- and 3 straight layers in y-direction (see Fig. S6).

2.4. Post processing

The UV-initiated crosslinking was conducted utilizing a UV light emitting diode device (Bluepoint, Dr. Hönle AG, Gräfelfing, Germany). The intensity was set to 130 $mWcm^{-2}$ at a stable distance of 5 cm and a wavelength of 300–600 nm. Each single sample was cross-linked using UV-irradiation at different angles (from above, from below and sideways) to assure a full light exposure of the fibres. In total, each sample was irradiated for 20 s.

2.5. Optical analysis

For the sinusoidal fibre morphology quantification of printed arrays, a set of measurement locations (n = 8) was chosen for n = 5 sample arrays using stereomicroscopy (Discovery V20, Carl Zeiss AG, Oberkochen, Germany). The resulting sinusoidal morphology was expressed as a peak-to-peak value and as wavelength. A detailed description and an example figure is provided in the Supplementary information (Figs. S3 and S4).

Scanning electron microscopy (SEM, Crossbeam 340 and Ultra Plus with GEMINI e-Beam column, Carl Zeiss AG Oberkochen, Germany) was used to visualize the printed fibres and scaffolds. The samples were sputter-coated with a 4 nm platinum layer prior to imaging.

2.6. Cytocompatibility testing

To assess the cytotoxicity, an eluate test based on DIN EN ISO 10993-5, −12 was conducted on the scaffolds prepared with PCLAC using the murine fibroblast cell line L929 CC1 (ATCC, Rockville, USA). A detailed description is provided in the Supplementary information. To study cell attachment behaviour on PCLAC scaffolds, human bone marrow-derived stromal cells (hMSCs) obtained from the femoral head of patients undergoing total hip arthroplasty were seeded on top of the biomaterial. These tests were performed in accordance with the Local Ethics Committee of the University of Würzburg, including informed consent from each donor. Located flattened on the well plate (Corning Costar, Sigma-Aldrich, Darmstadt, Germany) cells were seeded in a density of 120,000/scaffold (500 μL culture medium) on top of the scaffolds. After 24 h, 500 μL culture medium were added. Cells were cultured up to 14 days in DMEM F-12 (+1 vol.% Pen/Strep and +10 vol.% FCS) at 37 °C (5% CO_2/95% air). The culture medium was changed every three to four days. After 1, 7 and 14 days, the morphology of attached and spread hMSCs on PCLAC scaffolds was examined via live/dead-staining (LIVE/DEAD® Viability/Cytotoxicity Kit, for mammalian cells, Thermo Fisher Scientific Inc., Waltham, USA) using fluorescence microscopy. For these arrays, the scaffolds were placed in a new well plate, to exclude non adherent hMSCs from the staining. Positive cells detected after the staining were therefore definitely located within the scaffold and did not grow on the polystyrene well bottom.

2.7. Mechanical analysis

A low-force tensile tester (ElectroForce® 5500, Bose Corporation, Framingham, USA) with a 250 g load cell was used for single fibre tensile testing. A testing speed of 0.05 mm/s was used until failure. Furthermore, scaffolds with sinusoidal and straight patterns were tested with and without cyclic preloading at 10% strain and 1 Hz oscillation frequency for 10^4 testing cycles to assess the material resistance against creep. For these tests, specimens with 10 mm length and 5 mm width were prepared. Subsequently, the amount of fibre stacks was counted and multiplied with the corresponding cross-section. The cross-section of fibre stacks was then determined via stereomicroscopy of cut samples (n = 10, ImageJ, NIH).

To avoid plastic deformation during fibre preparation, the fibres were immersed in ethanol, detached from the collector surface and dried at environmental conditions. Afterwards, single fibres were mounted on cardboard frames and fixed by cyanoacrylate glue. The cardboard frame was cut after insertion in the mechanical testing device. While straight fibres exhibited a starting length of ε_0 = 3.0 mm, sinusoidal fibres were longer due to their crimped structure. Hence, the cross-sections and lengths of sinusoidal fibres were measured by stereomicroscopy imaging, analogous to the scaffolds, and considered as A_0 and ε_0 for tensile testing. The degree of the sinusoidal shape was provided as a percentage; e.g. 10% sinus indicates a 3.3 mm meandered fibre length on the card board frame length of 3.0 mm. To determine the fibre cross-section properly, example fibres were cut and characterized using SEM analysis. In addition, an elliptic fit was used to set the initial fibre area for mechanical testing and calculation of the tensile stress. For these tests, uniaxial scaffolds with sinusoidal and straight fibres were tensile tested. Here, n = 3 samples of each type were cyclically preloaded with 10^4 cycles, at 1 Hz oscillation and 10% tensile strain and compared to n = 3 samples as a reference. The determined Young's Moduli E_{x-y} are characterized by indices x−y representing the linear fitting range of the strain between x and y in per cent. All tests were performed at room temperature (22 ± 2 °C).

2.8. Statistical methods

Error bars in the study represent the sample standard deviation. At least n = 3 samples were used for presented experiments with listed error bars. The actual number of investigated samples is reported in the respective experimental sections. For statistical analysis, data groups were compared pairwise using a *t*-test with SigmaPlot (V12.5, Systat Software GmbH, Erkrath, Germany). The resulting statistical significance is reflected by the probability P in the Section 3.

3. Results

3.1. Copolymers for MEW

A summary of the physical and chemical properties of the copolymers is shown in Table 1 and the ^{1}H-NMR spectra for these two copolymers are presented in Figs. S1 and S2. The molar ratio of LLA/CL/AC in the final copolymer was close to the target ratio in each case. PCLAC exhibited a lower melting onset temperature; 55 °C versus 87 °C for PLACLAC. While the basic MEW performance of PLACLAC, including T_{min} = 145 °C at the nozzle and T_{res} = 130 °C at the melt reservoir, has been already demonstrated [22], the polymer PCLAC exhibited different printing characteristics. In the absence of lactide in the copolymer, a significantly decreased T_{min} = 105 °C and T_{res} = 90 °C was obtained, leading to stable and homogeneous fibre printing. As presented in Fig. 2, PCLAC copolymers could be deposited as fibres with fØ = 26.8 ± 1.9 μm and with a coefficient of variance CV = 7%, and accurately stacked by direct writing.

For both PLACLAC and PCLAC, a limited processing lifetime was observed, as the polymers slowly cross-linked in the melt reservoir during MEW. Nevertheless, the lifetime of PCLAC was considerably longer at t_{life} = 13 ± 7 h in contrast to PLACLAC with only t_{life} = 1.4 ± 0.7 h. In order to assess and compare changes in CTS and fØ during printing, the useful processing time was normalized as t_{norm}. The corresponding curves are given in Fig. 3. Here, t_{norm} = 1.0 is the end of the relative lifetime (relative means normalized to 1.0 or 100% respectively in this context) where the nozzle is finally blocked. Afterwards no sufficient *Taylor Cone* formation and thus, fibre formation could be achieved over the entire range of investigated feeding pressures: 0.3 bar ≤ p ≤ 4.0 bar.

As presented in Fig. 3A, the CTS of the PLACLAC jets increased gradually with time, starting at $0.01 \leq t_{norm} \leq 0.05$ with 135 ≤ CTS ≤ 315 mm/min, leading to peak values of 510 < CTS < 540 mm/min at p = 0.3 bar and 780 < CTS < 810 mm/min at p = 4.0 bar. After reaching this maximum at $0.5 < t_{norm} < 0.7$, the CTS followed a gradual decrease again.

In contrast to this result, the corresponding fØ decreased during the lifetime of the polymer, as shown in Fig. 3B. However, after an initial decrease from fØ ≈ 70 μm to fØ ≈ 55 μm at p = 4.0 bar or fØ ≈ 30 μm to fØ ≈ 20 μm at p = 0.3 bar respectively, a plateau-like zone was reached and maintained during $0.3 < t_{norm} < 0.7$. Afterwards, the fibre diameter decreased again until the printability finally ceased at t_{norm} = 1.0 by definition.

While each single isobar CTS-function of PCLAC exhibited similarities to PLACLAC, an opposite dependency between feeding pressure and CTS was observed. While increasingly faster PLACLAC jets with rising pressures were observed, PCLAC tended to slow down. Furthermore, the jet speed of PCLAC was more constant, only increasing by about 20% from the beginning towards the CTS maximum with 195 ≤ CTS ≤ 264 mm/min at $0.2 < t_{norm} < 0.4$.

Although both copolymers followed the same trend in changes of fibre diameter, only PCLAC could be printed with a high precision for a long period without blockage of the nozzle as t_{life} of PCLAC was significantly higher than PLACLAC. The CTS and fØ could be assumed as constant with small changes only during $0.1 < t_{norm} < 0.6$, leading to a useful MEW time interval of t = 7 ± 4 h for PCLAC high quality printing. Therefore, only PCLAC was used for the subsequent experiments.

3.2. Cytocompatibility

The cytotoxic effect of the PCLAC polymer on L929 cells was investigated by an eluate test as shown in Fig. 4. Eluates in different concentrations (100%, 50% and 25%) were added to the cells and viability/activity was evaluated compared to three controls: tissue culture polystyrene (PS) as positive control, polyvinylchloride (PVC) as negative control and PCL as reference biomaterial. For cell viability and activity, no significant differences were detected for the PCLAC polymer compared to PS. Since the measured absorbance and cell number are above 80% compared to PS, in accordance with the DIN EN ISO 10993-5, −12 the PCLAC polymer was classified as non-cytotoxic.

Cellular adhesion and spreading represent the initial phase of cell-scaffold interaction, which influences cellular proliferation and differentiation processes. In this study, adhesion of hMSCs on PCLAC scaffolds was determined using live/dead staining (Fig. 5). After 1 day in vitro (DIV), the cells were located directly

Table 1
Properties of the synthesized copolymers.

	Target molar ratio (LLA/CL/AC)	Actual molar ratio (LLA/CL/AC)	M_n (GPC) (Da)	$Đ_M$	T_g (°C)	T_m (°C)	ΔH_f (J/g)
PLACLAC	65/25/10	61/30/9	20,880	1.6	10	87	12.2
PCLAC	0/90/10	0/93/7	23,900	1.4	−52	48	62

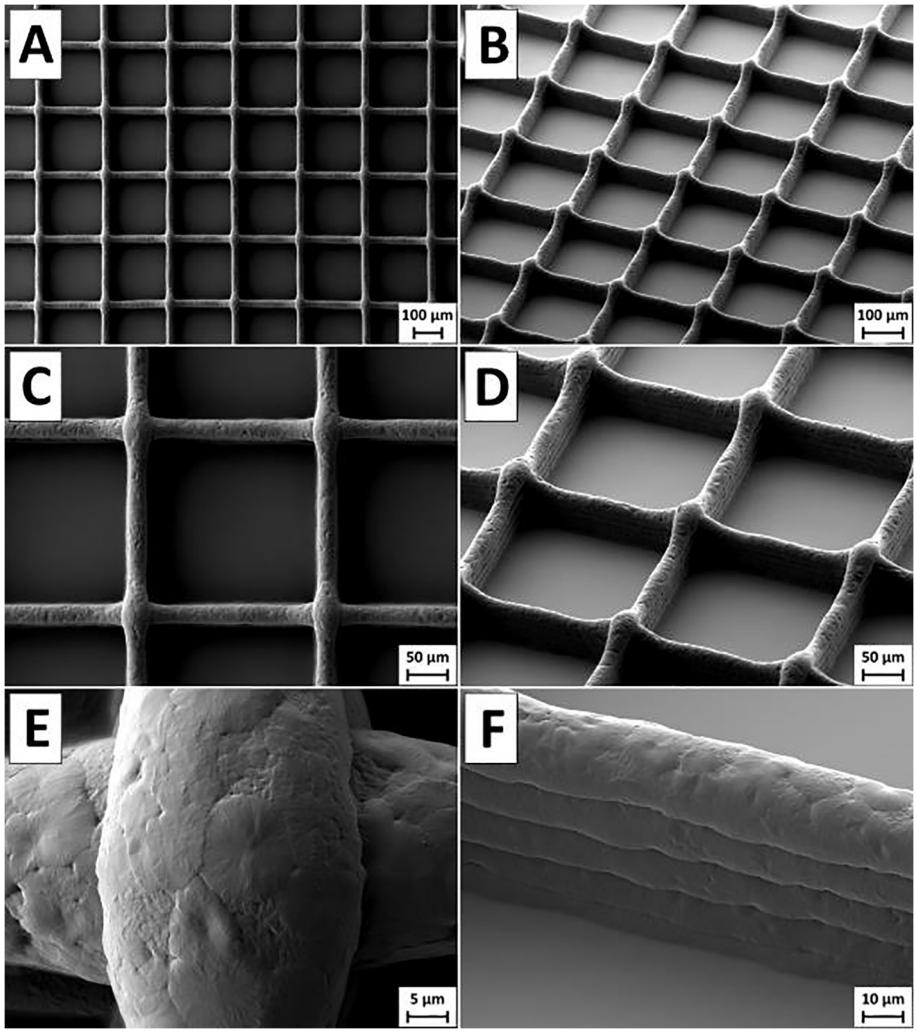

Fig. 2. SEM images of a PCLAC scaffold with 10 layers with 5 in both, x- and y-direction and 200 µm spacing could be deposited and stacked with high precision. (A–D) overview of the accurate scaffold structure. (E & F) The surface showed spherulites, as typical super-ordinated morphology characteristic of semi-crystalline polymers.

on the fibre surfaces without cell spreading in between the fibres (spacing = 300 µm). The cells showed high cell viability with proliferation behaviour throughout the culture period and formed a coherent network by bridging the spaces between the fibres on day 7 and 14.

3.3. Sinusoidal printing

Due to the improved lifetime of printing of PCLAC over PLACLAC, it was considered to be a suitable candidate for sub-CTS deposition as sinusoidal fibres. When a viscous fluid impinges a solid surface moving under proper conditions, different highly defined and reproducible patterns emerge [18]. Amongst these morphologies crimped patterns are particularly interesting as they have been demonstrated to be beneficial in generating extracellular matrix with biochemical composition similar to that of native ligament from bovine fibroblasts seeded onto the fibres [24]. As already shown elsewhere [21], PCL can be used for the MEW of such sinusoidal patterned fibres.

As shown in Fig. 6, the sinusoidal shape of the fibres can be adjusted by utilizing the collector speed. Here, homogeneous and stable printing conditions are very important, as fluctuations in the jet speed by pulsing [21] or crosslinking may lead to the deposition of disturbed patterns. However, while the resulting fibres were straight at CTS by definition, only sinusoidal meanders were observed at translation speeds (TS) of 65% < TS < 100% CTS. Above 100% of CTS, the sinusoidal shape disappeared as per definition. At slower collector speeds of TS = 68 ± 1% CTS, sinusoidal morphologies with maximum peak-to-peak values of 139 ± 17 µm and minimum wavelengths of 366 ± 39 µm could be processed under investigated conditions. More details on the printable morphology are provided in the Supplementary information.

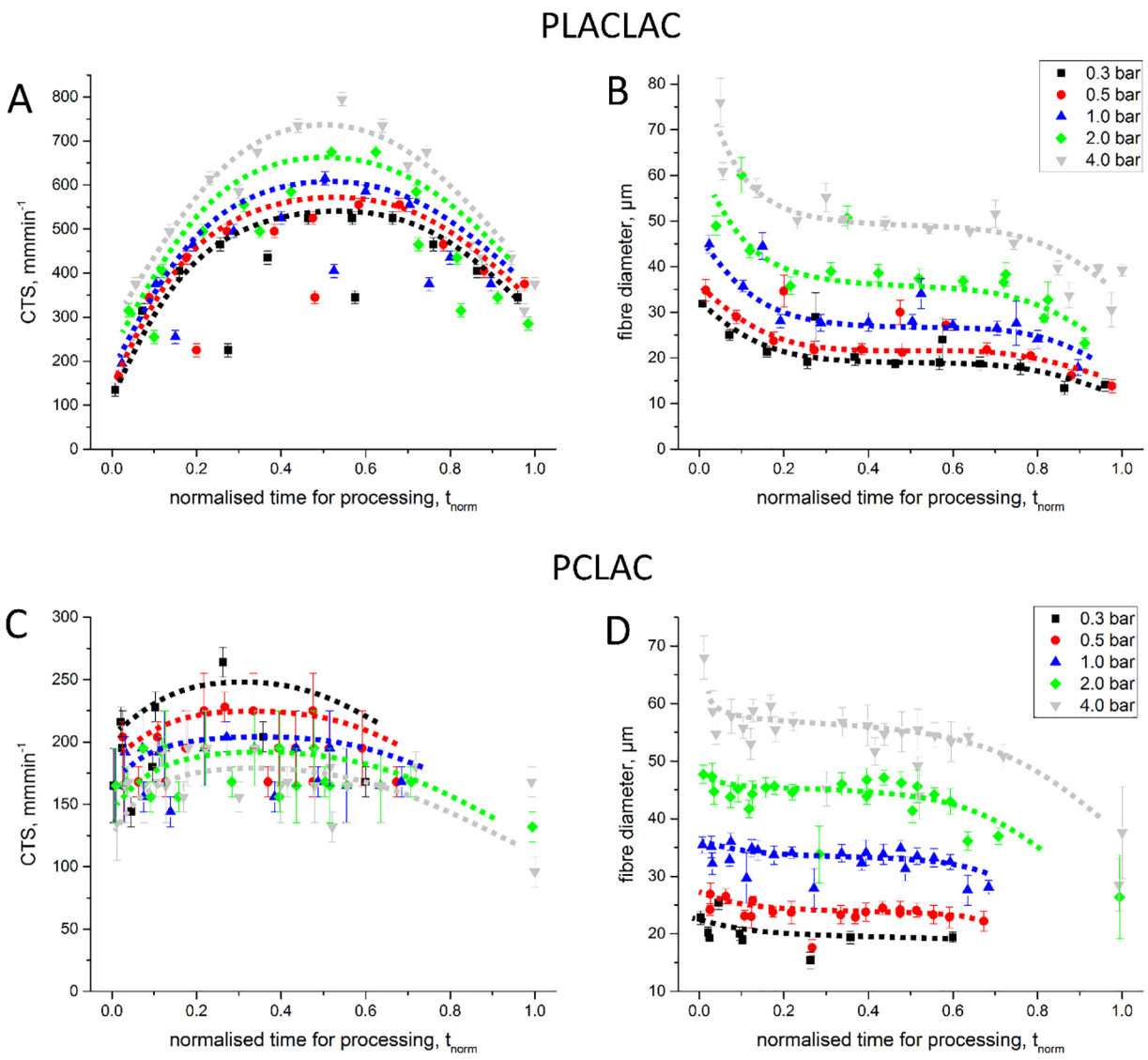

Fig. 3. CTS and fØ dependent on the polymers normalized time for processing. (A) CTS of PLACLAC, (B) fØ of PLACLAC, (C) CTS of PCLAC and (D) fØ of PCLAC. Spotted lines represent the general trend over time. While increased feeding pressures led to increased fibre diameters in both cases, higher pressures led to faster PLACLAC, but slower PCLAC jets.

3.4. Tensile properties of single fibres

Upon cross-linking, a change in T_g of the polymer occurs, from −52 °C (before cross-linking) to −42 °C (after cross-linking), while the degree of crystallinity, reflected in the ΔH_f, decreased; following crosslinking ΔH_f = 41.7 J/g and before cross-linking ΔH_f = 62 J/g (Table 1; Fig. S5). A dependency of the sinusoidal morphology and the resulting mechanical tensile properties could be observed as shown in Fig. 7. While straight fibres exhibited high Young's moduli at small strains, sinusoidal fibres with increasing peak-to-peak values exhibited a distinct toe region. Beyond this toe region, the crosslinked, crimped fibres change to a linear stress-strain response and a tensile modulus of $200 \geq E_{5-10} \geq 110$ MPa. Interestingly, the stiffness of the "sinus 10 ± 1%" samples with E_{0-2} = 79 ± 14 MPa and the "sinus 13 ± 1%" samples with E_{0-2} = 29 ± 17 MPa were remarkably different, emphasizing the distinct influence of already small morphological changes in the sinusoidal design. All three groups, straight, "sinus 10 ± 1%" and "sinus 13 ± 1%", exhibited a significant difference to the others with $P \leq 0.03$ at 0–2% strains. At 2–5% strain, straight fibres were significantly different compared to "sinus 10 ± 1%" with $P \leq 0.02$ and to "sinus 13 ± 1%" with $P \leq 0.003$. Despite the obvious difference in Young's moduli at small strains of ≤10% between straight fibres and sinusoidal fibres, both straight and sinusoidal fibres have similar maximum strength (~50 MPa) and elongation (~90%). The summarised tensile characteristics are presented in Table 2.

3.5. Tensile properties of sinusoidal fibre scaffolds

As presented in Fig. 8, the sinusoidal and straight scaffolds exhibited very similar stress-strain response as their corresponding single fibres. The sinusoidal scaffolds have a distinct toe region within the strain range of 0–0.1 mm/mm. Cyclic preloading (10^4 cycles, 1 Hz, 10% strain) further demonstrated the benefits of a cross-linked PCLAC elastomer. Indeed, the mechanical performance of the straight scaffolds decreased during preloading due to creep processes; however, they still exhibited a maximum tensile strength of σ_{max} = 20 ± 7 MPa.

In contrast to the straight scaffolds, no decrease in the mechanical performance of the sinusoidal scaffolds could be observed (comparison shown in Table 3). However, the maximum Young's modulus, strength and strain were smaller compared to the single fibres. This was a result of the sample conditions. While single fibres can be precisely aligned in the tensile tester, a certain

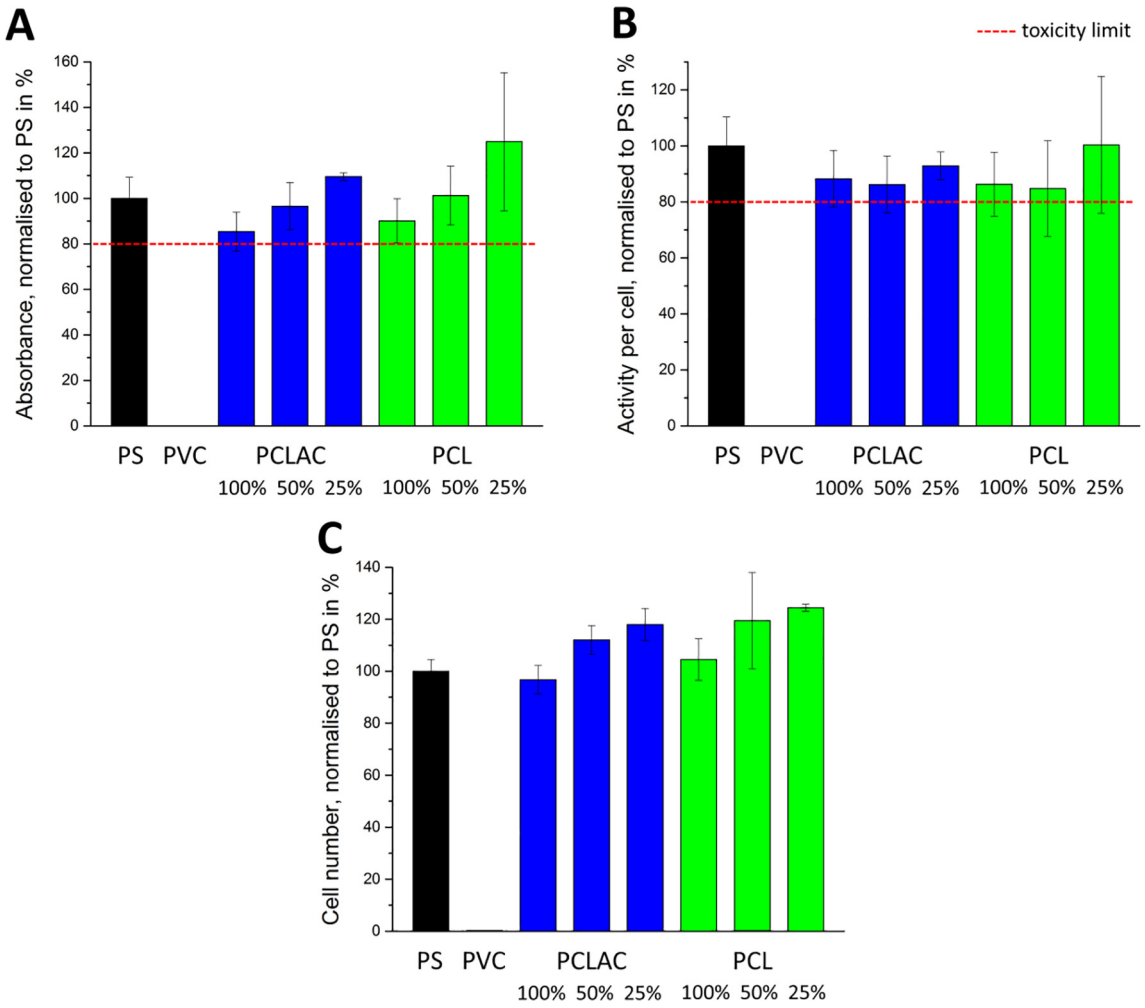

Fig. 4. Eluate test using L929 murine fibroblasts. (A) Absorbance, (B) activity per cell and (C) cell number compared to the PS and PVC control. After two days exposure, the UV-cross-linked PCLAC exhibited similar cytocompatibility to pure PCL.

amount of fibres in a scaffold network may be twisted and/or fail earlier than others, leading to an overall reduced maximum performance.

4. Discussion

4.1. Biomaterials approaches for ligament and tendon tissue engineering

Ligaments and tendons are complex tissues and to produce a functional and clinically relevant engineered replacement, a tissue-engineering scaffold must reflect this complexity. Despite the work done to date, no engineered ligament or tendon tissue has the appropriate extracellular architecture or mechanical properties leading to success following *in vivo* transplantation. One potential reason for this failure is the lack of scaffolds with a crimp architecture and mechanical properties capable of supporting tissue development *in vitro* and remodeling *in vivo.*

In early scaffold designs, knitting or braiding of the fibres was used to match the mechanical properties of the anterior cruciate ligament (ACL). With these approaches, many different polymers have been used, including natural (hyaluronan [25], silk [26,27] and type I collagen [28–30]) and biodegradable synthetic (poly (desamino tyrosyl-tryrosine ethyl ester carbonate)) [31], poly(L-lactide) (PLL) [32,33], poly(lactide-co-glycolide) (PLG) [34,35]) polymers. Type I collagen-based scaffolds have demonstrated excellent cellular adhesion, but lose their mechanical properties relatively quickly and are further limited by their potential immunogenicity and the high costs associated with purification [36,37]. Silk scaffolds have been prepared that have appropriate initial mechanical properties, and these scaffolds have been assessed in *in vivo* models. Chen et al. [38] used a scaffold consisting of braided silk fibres with collagen incorporation between the fibres. These scaffolds were seeded with bone marrow-derived mesenchymal stem cells, cultured for 5 days, and then implanted into a rabbit medial collateral ligament model. At 12 weeks, the newly developed tissue was less organized than the native tissue, was significantly weaker, possessing a modulus approximately half that of native medial collateral ligament, and had much smaller collagen fibril diameters. In a similar approach, Fan et al. employed a knitted silk mesh seeded and wrapped around a braided silk cord [39]. The internal silk chord was necessary to provide the appropriate mechanical properties. bone marrow-derived mesenchymal stem cells were seeded onto the scaffold and cultured overnight prior to implantation in a porcine model. When examined 24 weeks postoperatively, the engineered tissue was capable of carrying roughly half the load of native ACL, and the modulus was less than half that of native tissue. No quantitative assessment of tissue composition was reported, and the tissue did not possess crimped collagen fibrils or a toe region when tested in uniaxial tension.

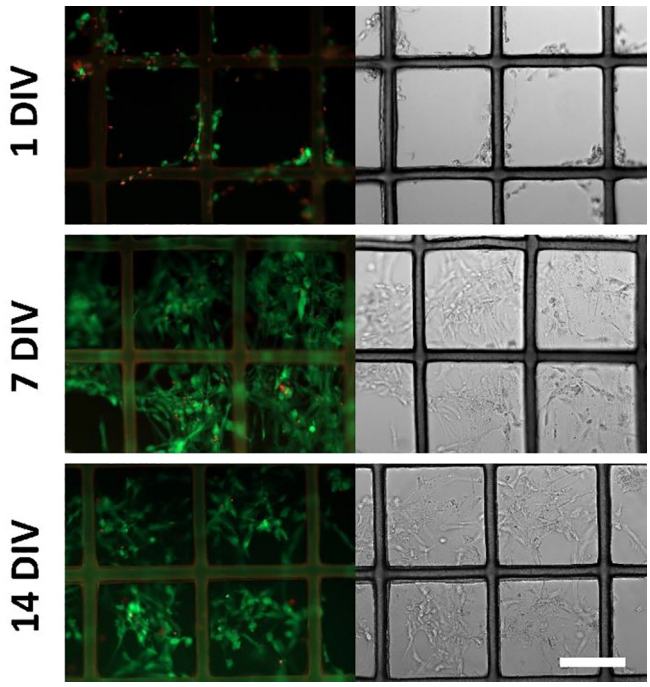

Fig. 5. hMSCs on PCLAC scaffolds. Representative fluorescence images (10× magnification) of cell adherence and morphology of hMSCs on PCLAC scaffolds after 1, 7 and 14 DIV. Green: live cells. Red: dead cells. Fibre spacing width = 300 μm, scale bar = 200 μm. (For interpretation of the references to colour in this figure legend, the reader is referred to the web version of this article.)

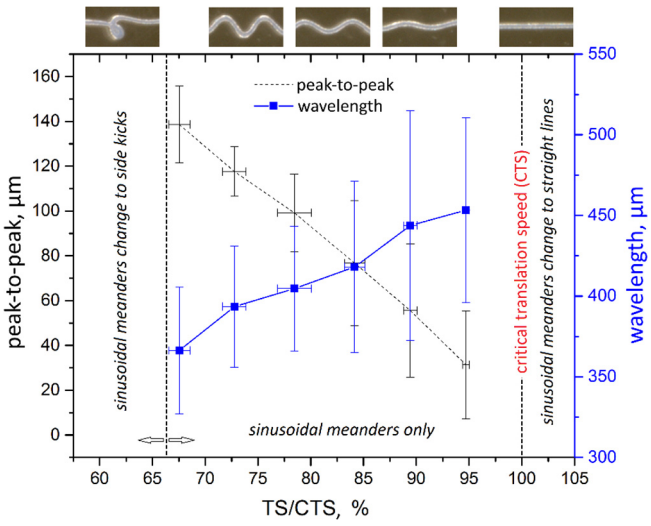

Fig. 6. Effect of the collector's translation speed (TS) on the printed fibre morphology of PCLAC. Below the CTS, sinusoidal patterns can be deposited. The resulting morphology can be varied through a slower speed leading to increased peak-to-peak values and reduced wavelength. Below 2/3 of CTS, different other patterns resulted. Printed at p = 1.0 bar.

In terms of approaches with synthetic polymers, uncross-linked degradable synthetic polyesters deform plastically and undergo fatigue failure under dynamic load, and thus do not possess appropriate mechanical properties. For example, fatigue failure was cited for the results of Cooper et al. [40] wherein scaffolds were prepared using braided PLLA fibres. These scaffolds were seeded with fibroblasts, cultured for 2 days, and implanted into a rabbit ACL model. At 4 weeks postoperatively, examination of the tissue showed that cells were primarily at the surface, with only limited cell penetration and minimal ECM deposition in the scaffold. By 12 weeks, the cells did penetrate to the centre of the scaffold. Nevertheless, these constructs exhibited no toe region and three of five of the implanted constructs had failed within the midsubstance region, and not at the bony interface. Thus, despite the work done to date, no engineered ligament or tendon tissue has the appropriate extracellular architecture or mechanical properties leading to success following *in vivo* transplantation.

In our previous studies, biodegradable polymers possessing the characteristic crimp pattern of the collagen fibrils in the ligament were generated via electrospinning [41]. This recreation of the microarchitecture of the ligament resulted in ACL fibroblasts producing ECM that was biochemically representative of that of the ligament and which spontaneously formed into collagen fibrils when cultured under dynamic conditions [42]. Furthermore, the ECM was accumulated at a greater rate than was accumulated on noncrimped polymer fibres. These findings have been supported by similar studies utilizing similarly crimped fibres prepared through electrospinning [43]. There is, therefore, clear advantage to using crimped fibrous scaffolds in ligament and tendon tissue engineering.

4.2. Copolymers for MEW

By omission of the lactide content in the copolymers, the T_{min} could be successfully decreased by about 40 °C, resulting in an extended MEW processing lifetime. Therefore, the time-range that led to almost constant CTS and fØ was sufficient ($t \approx 7 \pm 4$ h) for controlled printing. This enabled the fundamental conditions for controlled sinusoidal fibre deposition. However, besides other obvious advantages of a low printing temperature for the technical design of MEW devices, PCLAC fibres showed an outstanding stacking performance, similar to those of pure PCL. In contrast, no accurate stacking was observed for MEW of PLACLAC [22]. As presented, very regular fibre scaffolds could be manufactured. Here, the measured fØ = 26.8 ± 1.9 μm resulted in a CV = 7% only, indicating no adverse effects by fibre instabilities during MEW that were observed using PCL [21]. Hence, PCLAC showed improved MEW performance compared to PLACLAC.

However, the printing performance of PCLAC resembled that of PCL more so than did PLACLAC due to the CTS drop with increasing pressures. Why the PLACLAC jet speed increased with increasing pressures cannot be explained by the examined experiments. This finding is certainly interesting and may help to increase the printing speed significantly, but was out of the scope of the present study. Here, the role of lactide content and/or temperature with respect to charge density *etc.* will be the subject of further investigation.

4.3. Cytocompatibility

Eluate testing of the PCLAC polymer showed non-cytotoxic behaviour regarding DIN EN ISO 10993-5:2009, despite the utilized photo-initiator Irgacure 651 in the PCLAC. Williams et al. [44] found the photo-initiator Irgacure 651 to be highly toxic towards the hFOB cell line in hydrogel formation, with concentrations as low as 0.03% causing 100% cell death. For our experiments, we used highly concentrated Irgacure 651 (1 wt%) in the PCLAC polymer. Although some of the toxic-classified photo-initiator might be present in the fibre after cross-linking, there was no negative influence in cell viability detected, even at 100% eluate concentration. However, further analyses are necessary to determine the long-term effect on cytocompatibility during material degradation. In addition, it is conceivable to decrease the concentration of Irgacure 651 without changing the chemical properties of the PCLAC polymer or to use a different photo-initiator with less potential for toxic behaviour.

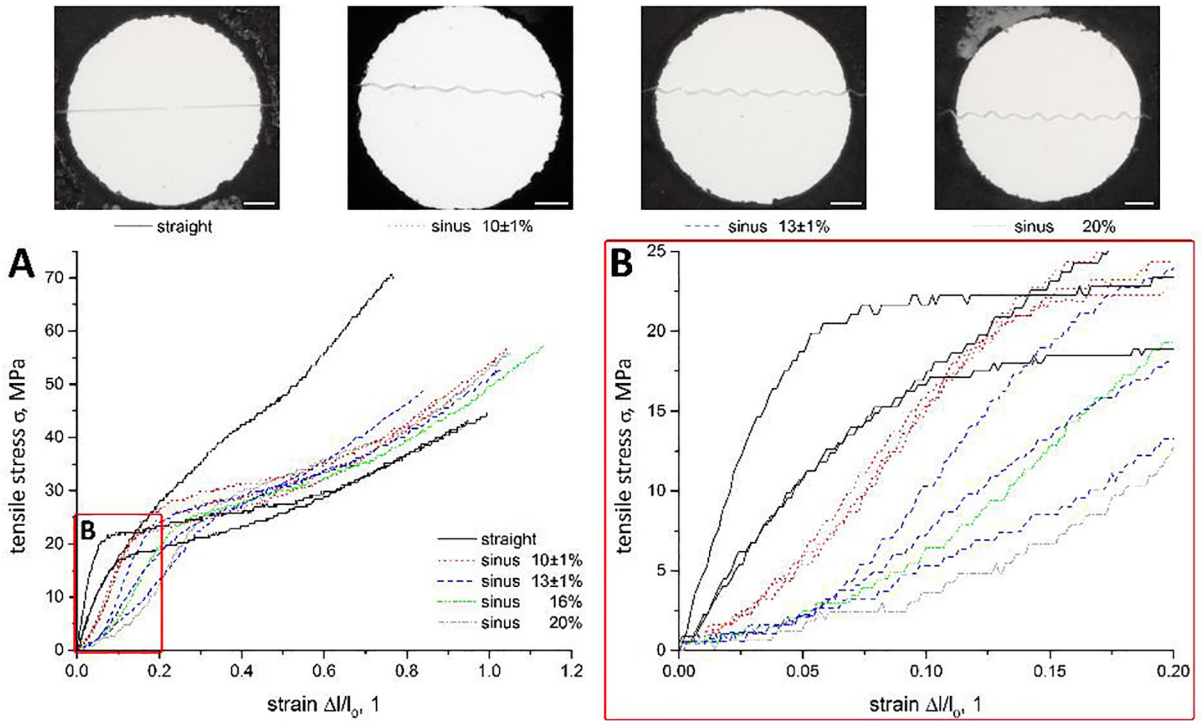

Fig. 7. Stress-strain curves of straight and sinusoidal PCLAC single fibres. The microscopic images visualize the differently pronounced sinusoids associated with the resulting tensile characteristics. While straight fibres exhibited no toe region, the fibre stiffness decreased significantly with more pronounced sinusoidal fibre shapes at small strains. (A) full stress-strain curves until rupture, (B) stress-strain curves at small strains only. The total length of a sinusoidal fibre is higher compared to a linear fibre, the percentage value characterizes this additional length.

Table 2
Tensile properties of PCLAC single fibres. The Young's moduli were obtained by linear fitting at the different strains intervals: 0–2%, 2–5% and 5–10%.

	Straight	Sinus 10 ± 1%	Sinus 13 ± 1%
E(0–2%), MPa	314 ± 157	79 ± 14	29 ± 17
E(2–5%), MPa	232 ± 51	137 ± 14	41 ± 6
E(5–10%), MPa	99 ± 41	200 ± 1	111 ± 53
σ_{max}, MPa	53 ± 16	51 ± 5	46 ± 9
ε_{max}, 1 (=mm/mm)	0.90 ± 0.12	0.95 ± 0.09	0.86 ± 0.17

4.4. Sinusoidal printing

Sinusoidal fibre shapes could be processed by reduction of the collector speed below the CTS of the melt jet. This approach uses linear movement and demands no further technical solutions and is therefore significantly easier to utilise than direct writing solutions that require more complex movement codes with a high axis precision and acceleration capability. Nevertheless, our approach to generate a sinusoidal shape of the deposited fibres is controllable by variation of the collector speed between 65% and 100% of CTS, ranging from very distinct sinusoids to linear fibres. However, it must be emphasized that the resulting sinusoidal features printed in this study exhibited wavelengths and peak-to-peak values in the range of tens to hundreds of micrometers which is not in accordance with the morphological size of crimped collagen fibrils in native tendon and ligament tissue. More appropriately the fibres printed in this study are of the size-scale for collagen fibres within native tissue [9].

4.5. Stress-strain behaviour

Our previous study showed that the stiffness of the poly(LLA-CL-AC) scaffolds increases significantly (up to ~10-fold) after

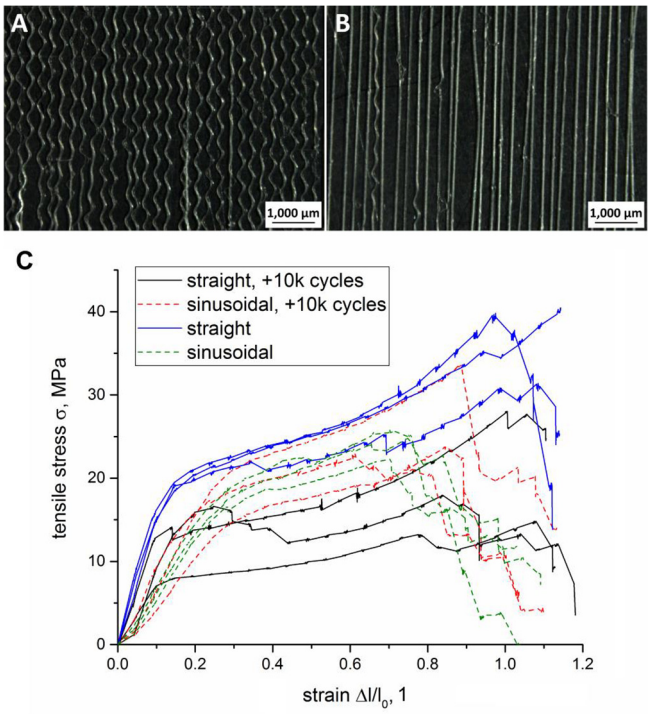

Fig. 8. Tensile testing of straight and sinusoidal scaffolds with and without cyclic preloading. (A) Microscopic image of a sinusoidal scaffold. (B) Microscopic image of a straight scaffold. Both scaffolds revealed the same fibre diameters with fø = 28.6 ± 3.6 µm. (C) While straight scaffolds decreased in their mechanical performance due to plastic material deformation, the sinusoidal scaffolds exhibited no differences after the cyclic preloading. All sinusoidal scaffolds show a clear toe region at small strains.

Table 3
Tensile properties of PCLAC scaffolds. The Young's moduli were obtained by linear fitting at 1–3% strain.

	Straight	Sinus 10 ± 3%
Without preload		
E(1–3%), MPa	170 ± 29	42 ± 16
σ_{max}, MPa	37 ± 5	24 ± 2
With preload; 10^4 cycles, 10%, 1 Hz		
E(1–3%), MPa	75 ± 51	47 ± 25
σ_{max}, MPa	20 ± 7	26 ± 7

cross-linking by UV irradiation at room temperature, compared with un-cross-linked microfiber scaffolds [22]. Similarly, in this study we found that post-process UV-curing resulted in significant increase in tensile strength, Young's modulus and creep resistance compared with un-cross-linked scaffolds, as un-crosslinked poly (CL-AC) samples even could not be handled without breakage.

In addition, the degree of the sinusoids exhibited a significant effect on the resulting stress-strain characteristics of both single fibres and entire scaffolds. While small peak-to-peak values led to short toe regions followed by stiff linear regions, distinct sinusoidal meanders underwent a more pronounced unfolding process and thus, revealed long toe regions with subsequent linear regions exhibiting a lower stiffness. For instance, the toe region of natural collagenous soft tissue usually covers 1–4% strain [1,13,45,46]. Promisingly, the tensile loading response of the investigated sinusoidal fibres and scaffolds was characteristic for, and in the range of, this qualitative mechanical response. With respect to the strain of natural tendon and ligament tissue, fibres with only slightly sinusoidal structuring might be already crimped enough for successful biomimetic behaviour.

However, sinusoidal scaffolds exhibited a clear improvement against straight scaffolds during cyclic fatigue testing. This improvement can be attributed to the geometry of the fibres. While the molecular chains of the straight fibres are constantly extended during pre-loading, slight creep or fatigue stress decrease with increasing loading cycle is quite normal for other, mostly thermoplastic, polymers. The sinusoidal scaffolds in contrast, change to straight morphology during cyclic pre-loading, leading to a reduced material fatigue. Beside the benefit of crimped patterns for maintaining the mechanical properties, the cross-link sites within or between fibres are believed to contribute to creep elimination and increases fibre tensile modulus and elasticity as the cross-link sites act as knots, locking the molecular chains and impeding sliding when exposed to dynamic stretching. The absence of significant creep of the sinusoidal scaffolds at 10% tensile strain during 10,000 cycles of loading is important, as it is known from literature that an elongation of only 6% (about 2 mm) of human ACL (about 32 mm long) is reported to be the limit beyond which damage must be expected [47].

5. Conclusion

In our study, we could demonstrate an approach to fabricate scaffolds that qualitatively mimic the biomechanical behaviour of tendon and ligament tissue. The polymer investigated here, p(ε-CL-co-AC), is cytocompatible and exhibited a good printing performance via MEW, with regular and homogenous fibres deposited onto a substrate. The p(ε-CL-co-AC) further showed excellent stacking behaviour properties and improved on the lifetime during printing compared to a previously investigated polymer, p(LLA-ε-CL-co-AC). Post-process UV-curing resulted in a high tensile strength as well as in a considerable Young's modulus, elasticity and creep resistance. By using collector speeds below the CTS, sinusoidal meanders comprised of fibers with few micrometres in diameter could be printed instead of straight fibres. Using this approach to structure entire sinusoidal scaffolds is a valuable tool for approximating the mechanical properties that result from the natural crimped structure of collagen type I fibrils in tendons and ligaments [13,48]. Thereby, the so-called toe region during tensile load can be not only achieved, but also tuned at relevant strains. Hence, sinusoidal MEW of p(ε-CL-co-AC) by direct-writing below the CTS can be considered as promising approach for tendon and ligament tissue engineering.

Acknowledgements

This work was supported by the European Research Council (ERC) (consolidator grant Design2Heal, contract number 617989), by the Natural Sciences and Engineering Research Council of Canada (RGPIN/05179-2015) and by the German Research Foundation (DFG) ("State Major Instrumentation Programme", funding for the scanning electron microscope Zeiss Crossbeam 340, INST 105022/58-1 FUGG). The authors thank the orthopaedic department (Profs. Max Rudert and Franz Jakob) of the university of Würzburg for supplying the hMSC cells and Phillipp Stahlhut for help with SEM.

Declaration of interests

The authors declare no conflict of interests.

Appendix A. Supplementary data

Supplementary data associated with this article can be found, in the online version, at https://doi.org/10.1016/j.actbio.2018.03.023.

References

[1] G. Walden, X. Liao, S. Donell, M.J. Raxworthy, G.P. Riley, A. Saeed, A. Clinical, Biological, and biomaterials perspective into tendon injuries and regeneration, Tissue Eng. Part B Rev. 23 (1) (2017) 44–58.
[2] R.V. West, C.D. Harner, Graft selection in anterior cruciate ligament reconstruction, J. Am. Acad. Orthopaedic Surgeons 13 (3) (2005) 197–207.
[3] A.A. Macaulay, D.C. Perfetti, W.N. Levine, Anterior cruciate ligament graft choices, Sports Health A Multidiscipl. Approach 4 (1) (2012) 63–68.
[4] C.K. Kuo, J.E. Marturano, R.S. Tuan, Novel strategies in tendon and ligament tissue engineering: advanced biomaterials and regeneration motifs, BMC Sports Science, Med. Rehabil. 2 (1) (2010) 20.
[5] M.L. Santos, M.T. Rodrigues, R.M. Domingues, R.L. Reis, M.E. Gomes, Biomaterials as Tendon and Ligament Substitutes: Current Developments, Regenerative Strategies for the Treatment of Knee Joint Disabilities, Springer, 2017, pp. 349–371.
[6] S. Sahoo, H. Ouyang, J.C.-H. Goh, T. Tay, S. Toh, Characterization of a novel polymeric scaffold for potential application in tendon/ligament tissue engineering, Tissue Eng. 12 (1) (2006) 91–99.
[7] Y. Liu, H. Ramanath, D.-A. Wang, Tendon tissue engineering using scaffold enhancing strategies, Trends Biotechnol. 26 (4) (2008) 201–209.
[8] A.B. Youssef, S.J. Hollister, P.D. Dalton, Additive manufacturing of polymer melts for implantable medical devices and scaffolds, Biofabrication 9 (1) (2017) 012002.
[9] J.G. Snedeker, J. Foolen, Tendon injury and repair – A perspective on the basic mechanisms of tendon disease and future clinical therapy, Acta Biomater. 63 (Supplement C) (2017) 18–36.
[10] A. Hoffmann, G. Gross, Tendon and ligament engineering in the adult organism: mesenchymal stem cells and gene-therapeutic approaches, Int. Orthop. 31 (6) (2007) 791–797.
[11] P. Sharma, N. Maffulli, Biology of tendon injury: healing, modeling and remodeling, J. Musculoskelet. Neuronal Interact. 6 (2) (2006) 181.
[12] C.T. Laurencin, J.W. Freeman, Ligament tissue engineering: an evolutionary materials science approach, Biomaterials 26 (36) (2005) 7530–7536.
[13] J.H.-C. Wang, Mechanobiology of tendon, J. Biomech. 39 (9) (2006) 1563–1582.
[14] P.D. Dalton, Melt electrowriting with additive manufacturing principles, Curr. Opin. Biomed. Eng. 2 (2017) 49–57.
[15] T.D. Brown, P.D. Dalton, D.W. Hutmacher, Direct writing by way of melt electrospinning, Adv. Mater. 23 (47) (2011) 5651–5657.
[16] G. Hochleitner, T. Jungst, T.D. Brown, K. Hahn, C. Moseke, F. Jakob, P.D. Dalton, J. Groll, Additive manufacturing of scaffolds with sub-micron filaments via melt electrospinning writing, Biofabrication 7 (3) (2015) 035002.

[17] T. Jungst, M.L. Muerza-Cascante, T.D. Brown, M. Standfest, D.W. Hutmacher, J. Groll, P.D. Dalton, Melt electrospinning onto cylinders: effects of rotational velocity and collector diameter on morphology of tubular structures, Polym. Int. 64 (9) (2015) 1086–1095.
[18] P.T. Brun, B. Audoly, N.M. Ribe, T.S. Eaves, J.R. Lister, Liquid ropes: a geometrical model for thin viscous jet instabilities, Phys. Rev. Lett. 114 (17) (2015) 174501.
[19] S.W. Morris, J.H.P. Dawes, N.M. Ribe, J.R. Lister, Meandering instability of a viscous thread, Phys. Rev. E 77 (6) (2008) 066218.
[20] S. Chiu-Webster, J.R. Lister, The fall of a viscous thread onto a moving surface: a 'fluid-mechanical sewing machine', J Fluid Mech. 569 (2006) 89–111.
[21] G. Hochleitner, A. Youssef, A. Hrynevich, J.N. Haigh, T. Jungst, J. Groll, P.D. Dalton, Fibre pulsing during melt electrospinning writing, BioNanoMaterials 17 (3–4) (2016) 159–171.
[22] F. Chen, G. Hochleitner, T. Woodfield, J. Groll, P.D. Dalton, B.G. Amsden, Additive manufacturing of a photo-cross-linkable polymer via direct melt electrospinning writing for producing high strength structures, Biomacromolecules 17 (1) (2016) 208–214.
[23] F. Chen, J.W. Hayami, B.G. Amsden, Electrospun poly (l-lactide-co-acryloyl carbonate) fiber scaffolds with a mechanically stable crimp structure for ligament tissue engineering, Biomacromolecules 15 (5) (2014) 1593–1601.
[24] D.C. Surrao, J.C. Fan, S.D. Waldman, B.G. Amsden, A crimp-like microarchitecture improves tissue production in fibrous ligament scaffolds in response to mechanical stimuli, Acta Biomater. 8 (10) (2012) 3704–3713.
[25] S. Cristino, F. Grassi, S. Toneguzzi, A. Piacentini, B. Grigolo, S. Santi, M. Riccio, E. Tognana, A. Facchini, G. Lisignoli, Analysis of mesenchymal stem dimensional HYAFF 11 (R)-based cells grown on a prototype ligament scaffold, J. Biomed. Mater. Res. Part A 73A (2005) 275–283.
[26] G.H. Altman, R.L. Horan, H.H. Lu, J. Moreau, I. Martin, J.C. Richmond, D.L. Kaplan, Silk matrix for tissue engineered anterior cruciate ligaments, Biomaterials 23 (2002) 4131–4141.
[27] X. Li, J.G. Snedeker, Wired silk architectures provide a biomimetic ACL tissue engineering scaffold, J. Mech. Behav. Biomed. Mater. 22 (2013) 30–40.
[28] U. Noth, K. Schupp, A. Heymer, S. Kall, F. Jakob, N. Schutze, B. Baumann, T. Barthel, J. Eulert, C. Hendrich, Anterior cruciate ligament constructs fabricated from human mesenchymal stem cells in a collagen type I hydrogel, Cytotherapy 7 (2005) 447–455.
[29] E. Gentleman, A.N. Lay, D.A. Dickerson, E.A. Nauman, G.A. Livesay, K.C. Dee, Mechanical characterization of collagen fibers and scaffolds for tissue engineering, Biomaterials 24 (2003) 3805–3813.
[30] M. Chvapil, D. Speer, H. Holubec, T. Chvapil, D. King, Collagen-fibers as a temporary scaffold for replacement of ACL in goats, J. Biomed. Mater. Res. 27 (1993) 313–325.
[31] N. Tovar, S. Bourke, M. Jaffe, N.S. Murthy, J. Kohn, C. Gatt, M.G. Dunn, A comparison of degradable synthetic polymer fibers for anterior cruciate ligament reconstruction, J. Biomed. Mater. Res. Part A 93A (2010) 738–747.
[32] L. Durselen, M. Dauner, H. Hierlemann, H. Planck, A. Ignatius, L. Claes, Control of material stiffness during degradation for constructs made of absorbable polymer fibers, J. Biomed. Mater. Res. B 67B (2003) 697–701.
[33] J.A. Cooper Jr, L. Bailey, J.N. Carter, C.E. Castiglioni, Evaluation of the anterior cruciate ligament, medial collateral ligament, achilles tendon and patellar tendon as cell sources for tissue-engineered ligament, Biomaterials (2006).
[34] F. van Eijk, D.B.F. Saris, J. Riesle, W.J. Willems, C.A. van Blitterswijk, A.J. Verbout, W.J. Dhert, Tissue engineering of ligaments: a comparison of bone marrow stromal cells, Anterior Cruciate Ligament, and Skin Fibroblasts as Cell Source, Tissue Eng. 10 (2004) 893–903.
[35] S. Sahoo, H. Ouyang, J. Goh, T.E. Tay, S.L. Toh, Characterization of a novel polymeric scaffold for potential application in tendon/ligament tissue engineering, Tissue Eng. 12 (2006) 91–99.
[36] F.A. Petrigliano, D.R. McAllister, B.M. Wu, Tissue engineering for anterior cruciate ligament reconstruction: a review of current strategies, Arthroscopy 22 (2006) 441–451.
[37] S.J. Kew, J.H. Gwynne, D. Enea, M. Abu-Rub, A. Pandit, D. Zeugolis, R.A. Brooks, N. Rushton, S.M. Best, R.E. Cameron, Regeneration and repair of tendon and ligament tissue using collagen fibre biomaterials, Acta Biomater. 7 (2011) 3237–3247.
[38] X. Chen, Y.Y. Qi, L.L. Wang, Z. Yin, G.L. Yin, X.H. Zou, Ligament regeneration using a knitted silk scaffold combined with collagen matrix, Biomaterials (2008).
[39] H. Fan, H. Liu, S.L. Toh, J.C.H. Goh, Anterior cruciate ligament regeneration using mesenchymal stem cells and silk scaffold in large animal model, Biomaterials 30 (2009) 4967–4977.
[40] J.A. Cooper, J.S. Sahota, W.J. Gorum, J. Carter, S.B. Doty, C.T. Laurencin, Biomimetic tissue-engineered anterior cruciate ligament replacement, Proc. Natl. Acad. Sci. U.S.A. 104 (2007) 3049–3054.
[41] D.C. Surrao, J.W.S. Hayami, S.D. Waldman, B.G. Amsden, Self-crimping, biodegradable, electrospun polymer microfibers, Biomacromolecules 11 (2010) 3624–3629.
[42] D.C. Surrao, J.C.Y. Fan, S.D. Waldman, B.G. Amsden, A crimp-like microarchitecture improves tissue production in fibrous ligament scaffolds in response to mechanical stimuli, Acta Biomater. 8 (2012) 3704–3713.
[43] P.-H. Grace Chao, H.-Y. Hsu, H.-Y. Tseng, Electrospun microcrimped fibers with nonlinear mechanical properties enhance ligament fibroblast phenotype, Biofabrication 6 (2014) 035008.
[44] C.G. Williams, A.N. Malik, T.K. Kim, P.N. Manson, J.H. Elisseeff, Variable cytocompatibility of six cell lines with photoinitiators used for polymerizing hydrogels and cell encapsulation, Biomaterials 26 (11) (2005) 1211–1218.
[45] K.A. Hansen, J.A. Weiss, J.K. Barton, Recruitment of tendon crimp with applied tensile strain, Trans. Am. Soc. Mech. Eng. J. Biomech. Eng. 124 (1) (2002) 72–77.
[46] Y. Wu, B. Wu, S. Vijayavenkataraman, Y. San Wong, J.Y.H. Fuh, Crimped fiber with controllable patterns fabricated via electrohydrodynamic jet printing, Mater. Des. (2017).
[47] A.A. Amis, G.P.C. Dawkins, Functional anatomy of the anterior cruciate ligament: fiber bundle actions related to ligament replacements and injuries, J. Bone Joint Surg. 73-B (1991) 260e7.
[48] A.D. Freed, T.C. Doehring, Elastic model for crimped collagen fibrils, J. Biomech. Eng. 127 (4) (2005) 587–593.